sites in a non-recombining chromosome, and more theoretical work is needed. □

Methods

We used the sequences of *SLX-1* and *SLY-1* to design the following primers for the polymerase chain reaction (PCR) and sequencing (Fig. 1): '–7', 5′-ACTTGCAACG ACTTCACTTTGAG-3′; '–8', 5′-ATCGAATTCCAGTGGAAGTCCA-3′; '+11', 5′-AAGCTCACAATGCTGATCTTC-3′; '+9', 5′-GCTGAAGATGGCTTGCTAAAC-3′; '+6', 5′-TGGACTTCCACTGGAATTCGAT-3′; '–10', 5′-TCCAGCAGAGCTTGAACAGTC-3′.

A standard cetyltrimethylammonium bromide plant miniprep method with several modifications[28] was used to isolate the total genomic DNA from 12 *S. latifolia* males and from 17 plants (2 parents, 10 sons and 5 daughters) used in the *SLX-1* segregation analysis. The 2-kb 3′ region in 12 *S. latifolia* males was amplified using the following primer pairs: '+11' and '–7' for *SLX-1*; '+11' and '–8' for *SLY-1*. Because we studied sequences from the X and Y chromosomes of males, direct sequencing was possible for all individuals. Amplification products were passed through 1% agarose gels, column-purified (Qiagen gel extraction kit) and sequenced with the primers listed above, using an ABI Prism 377 automatic sequencer (Perkin Elmer).

The primer pair '+6' and '–7' was used to amplify the short (0.6 kb) 3′ *SLX-1* region used in the *SLX-1* segregation analysis. PCR products of both parents were directly sequenced and these sequences were used to choose a restriction enzyme (*Hpa*I) to cut the PCR product of only one of the parents. The restriction site was used as a molecular genetic marker in the *SLX-1* segregation analysis.

For the coalescent simulations, we used the program ProSeq v.2.4 (D. Filatov, unpublished, available at http://helios.bto.ed.ac.uk/evolgen/filatov/proseq.html). All simulations assumed zero recombination. Simulations to estimate the significance of the lack of diversity in the *SLY-1* gene were conditioned on the observed numbers of segregating sites. Simulations with a selective sweep were conducted according to ref. 29. The neighbour-joining tree was constructed using MEGA software[30], based on pairwise divergence values, with Jukes-Cantor correction.

Received 19 August 1999; accepted 28 January 2000.

1. Bull, J. J. *Evolution of Sex Determining Mechanisms*. (Benjamin/Cummings, Menlo Park, 1993).
2. Charlesworth, B. The evolution of chromosomal sex determination and dosage compensation. *Curr. Biol.* **6,** 149–162 (1996).
3. Rice, W. R. Genetic hitchhiking and the evolution of reduced genetic activity of the Y sex chromosome. *Genetics* **116,** 161–167 (1987).
4. Manning, J. T. & Thompson, D. J. Muller's ratchet and the accumulation of favourable mutations. *Acta Biotheoretica* **33,** 219–225 (1984).
5. Charlesworth, D., Charlesworth, B. & Morgan, M. T. The pattern of neutral molecular variation under the background selection model. *Genetics* **141,** 1619–1632 (1995).
6. Orr, H. A. & Kim, Y. An adaptive hypothesis for the evolution of the Y chromosome. *Genetics* **150,** 1693–1698 (1998).
7. Delichère, C. *et al.* SlY1, the first active gene cloned from a plant Y chromosome encodes a WD-repeat protein. *EMBO J.* **18,** 4169–4179 (1999).
8. Grant, S. *et al.* Genetics of sex determination in flowering plants. *Dev. Genet.* **15,** 214–230 (1994).
9. Westergaard, M. The mechanism of sex determination in dioecious flowering plants. *Adv. Genet.* **9,** 217–281 (1959).
10. Desfeux, C. *et al.* Evolution of reproductive systems in genus *Silene*. *Proc. R. Soc. Lond. B.* **263,** 409–414 (1996).
11. Anagnostopoulos, T., Green, P. M., Rowley, G., Lewis, C. M. & Giannelli, F. DNA variation in a 5-Mb region of the X-chromosome and estimates of sex-specific/type-specific mutation rates. *Am. J. Hum. Genet.* **64,** 508–517 (1999).
12. Burrows, W. & Ryder, O. A. Y-chromosome variation in great apes. *Nature* **385,** 125–126 (1997).
13. Lundrigan, B. L. & Tucker, P. K. Tracing paternal ancestry in mice, using the Y-linked sex-determining locus *Sry*. *Mol. Biol. Evol.* **11,** 483–492 (1994).
14. Nachman, M. W. & Aquadro, C. F. Polymorphism and divergence at the 5′ flanking region of the sex determining locus, *Sry*, in mice. *Mol. Biol. Evol.* **11,** 539–547 (1994).
15. Zurovcova, M. & Eanes, W. F. Lack of nucleotide polymorphism in the Y-linked sperm flagellar dynein gene *Dhc-Yh3* of *Drosophila melanogaster* and *D.* simulans. *Genetics* **153,** 1709–1715 (1999).
16. McAllister, B. & Charlesworth, B. Reduced sequence variability on the neo-Y chromosome of *Drosophila americana americana*. *Genetics* **153,** 221–233 (1999).
17. Ye, D. *et al.* Sex determination in the dioecious *Melandrium*. I. First lessons from androgenic haploids. *Sex. Plant Reprod.* **3,** 179–186 (1990).
18. Vagera, J., Paulikova, D. & Dolezel, J. The development of male and female regenerants by *in vitro* Androgenesis in dioecious plant *Melandrium album*. *Ann. Botany* **73,** 455–459 (1994).
19. Bùzek, J. *et al.* Isolation and characterization of X chromosome-derived DNA sequences from a dioecious plant *Melandrium album*. *Chromosome Res.* **5,** 57–65 (1997).
20. Guttman, D. S. & Charlesworth, D. An X-linked gene with a degenerate Y-linked homologue in a dioecious plant. *Nature* **393,** 263–265 (1998).
21. Nei, M. *Molecular Evolutionary Genetics*. (Columbia Univ. Press, New York, 1987).
22. Hudson, R. R. & Kaplan, N. L. Statistical properties of the number of recombination events in the history of a sample of DNA sequences. *Genetics* **111,** 147–164 (1985).
23. Hudson, R. R. Estimating the recombination parameter of a finite population model without selection. *Genet. Res.* **50,** 245–250 (1987).
24. Gaut, B. S. Molecular clocks and nucleotide substitution rates in higher plants. *Evol. Biol.* **30,** 93–120 (1998).
25. Hudson, R. R. Gene genealogies and the coalescent process. *Oxf. Surv. Evol. Biol.* **7,** 1–44 (1990).
26. Fu, Y. -X. & Li, W.-H.Statistical tests of neutrality of mutations. *Genetics* **133,** 693–709 (1993).
27. Tajima, F. Statistical method for testing the neutral mutation hypothesis by DNA polymorphism. *Genetics* **123,** 585–595 (1989).
28. Filatov. D. A. & Charlesworth, D. DNA polymorphism, haplotype structure and balancing selection in the Leavenworthia PgiC locus. *Genetics* **153,** 1423–1434 (1999).
29. Braverman, J. M., Hudson, R. R., Kaplan, N. L., Langley, C. H. & Stephan, W. The hitchhiking effect on the site frequency spectrum of DNA polymorphism. *Genetics* **140,** 783–796 (1995).
30. Kumar, S., Tamura, K. & Nei, M. *MEGA: Molecular Evolutionary Genetics Analysis, version 1.0*. (Pennsylvania State Univ., Univ. Park, 1993).

Acknowledgements

We thank M. Turelli and B. Charlesworth for discussions and advice. D.C. was supported by the Natural Environment Research Council of Great Britain, D.A.F. by a grant from the Leverhulme Trust, and F.M. and I.N. by research contracts from the Centre National de la Recherche Scientifique, the Institut National de la Recherche Agrononique and the Ecole Normale Supérieure of France.

Correspondence and requests for materials should be addressed to D.C. (e-mail: Deborah.Charlesworth@ed.ac.uk).

Representation of a perceptual decision in developing oculomotor commands

Joshua I. Gold & Michael N. Shadlen

Department of Physiology and Biophysics, and Regional Primate Research Center, University of Washington, Seattle, Washington 98195-7290, USA

Behaviour often depends on the ability to make categorical judgements about sensory information acquired over time. Such judgements require a comparison of the evidence favouring the alternatives[1–4], but how the brain forms these comparisons is unknown. Here we show that in a visual discrimination task, the accumulating balance of sensory evidence favouring one interpretation over another is evident in the neural circuits that generate the behavioural response. We trained monkeys to make a direction judgement about dynamic random-dot motion[5] and to indicate their judgement with an eye movement to a visual target. We interrupted motion viewing with electrical microstimulation of the frontal eye field and analysed the resulting, evoked eye movements for evidence of ongoing activity associated with the oculomotor response[6–10]. Evoked eye movements deviated in the direction of the monkey's judgement. The magnitude of the deviation depended on motion strength and viewing time. The oculomotor signals responsible for these deviations reflected the accumulated motion information that informed the monkey's choices on the discrimination task. Thus, for this task, decision formation and motor preparation appear to share a common level of neural organization.

The difficulty of the direction discrimination task (Fig. 1a, b) depended on the percentage of coherently moving random dots and the amount of time that the monkey was given to view the motion stimulus. At high motion strengths, the monkey can make an accurate direction judgement in a short time. In contrast, when the stimulus is close to the psychophysical threshold, the monkey must base its direction judgement on weak motion signals interpreted over a longer period of time[5]. These judgements are thought to involve the accumulation of motion information represented in the extrastriate visual cortex[11]. This accumulated motion information ultimately guides selection of the eye-movement response. The fact that the monkey knows beforehand which eye movement it must make to indicate a particular direction judgement suggests that, for this task, its decision can be formed by an ongoing conversion of motion information directly into an appropriate oculomotor command. We tested this idea by using electrically evoked eye movements to assess the influence of motion strength and viewing duration on oculomotor commands that develop

while the monkey is viewing the dots and forming its direction judgement.

We began microstimulation of the frontal eye field (FEF) simultaneously with offset of the motion stimulus and the fixation point, which typically resulted in two, temporally separable eye movements (Fig. 1c–e). The first, electrically evoked movement began 44 ± 10 ms (mean ± s.d.; 37,611 trials) after the fixation-point offset. This movement probably began before the oculomotor system received the signal to move the eyes voluntarily, as visual latencies exceed 60 ms in the FEF[12] and 40–50 ms in the deep layers of the superior colliculus[13,14]. The eyes then remained relatively stationary for 95 ± 32 ms, which allowed reliable measurement of the endpoint position of the electrically evoked saccade. The second, voluntary movement began 171 ± 33 ms after fixation-point offset and travelled from the endpoint of the evoked saccade to one of the two choice targets, thereby indicating the monkey's direction judgement.

Eye movements evoked by electrical microstimulation of the FEF during the discrimination task depended on the monkey's subsequent direction judgement. For the experiment depicted in Fig. 2a, the endpoints of all electrically evoked saccades were to the right of the fixation point. However, on trials in which the monkey subsequently chose the upper target, the endpoints of the evoked saccades tended to deviate upwards (filled symbols). Conversely, on trials in which the monkey chose the lower target, the endpoints tended to deviate downwards (open symbols). For all 27 sites tested, saccades evoked on discrimination trials were similar to those evoked with fixation but tended to deviate in the direction of the subsequently selected target. As shown in Fig. 2b and c, the angle describing this saccade deviation did not differ substantially from the angle defined by the choice targets (mean angular difference ± s.e.m., 2.8 ± 3.5°; paired *t*-test, $P = 0.43$). This result indicates that the trajectory of the electrically evoked saccade was determined by both the site of stimulation and a developing oculomotor command towards the choice target, in a manner consistent with a vector-averaging procedure[15–17].

In any one experiment, electrically evoked saccades deviated in the direction of the subsequently selected target by variable amounts (Fig. 2a). The magnitude of this deviation depended on the fraction of coherently moving random dots and the amount of viewing time. Figure 3a shows the endpoints of evoked saccades on trials from a single experiment in which weak motion was presented for a short time, conditions that make it difficult to reach an accurate direction judgement. These evoked saccades varied only weakly with target choice. In contrast, when strong motion was presented for a longer time, evoked saccades from the same site were clearly separated as a function of target choice (Fig. 3b).

The effect of coherence and viewing duration was evident across the population of 37,611 trials from 27 stimulation sites. For each trial, we determined the component of the electrically evoked saccade in the direction of the choice target. On average, this quantity increased in magnitude with increasing motion strength (Fig. 3c; the effect of motion strength was significant for all but the earliest epoch: linear regression, *F* test, $P < 0.01$) and increasing viewing duration (Fig. 3d; the effect of viewing duration was

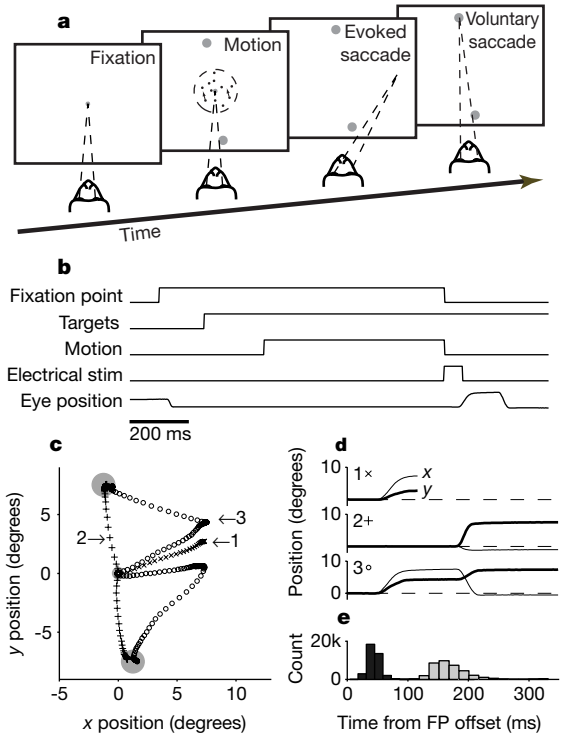

Figure 1 Microstimulation paradigm. **a**,**b**, After the monkey fixated, two choice targets appeared 8° from the fixation point. The motion stimulus then appeared after 100–600 ms and remained on for 100–1,100 ms, until fixation-point offset. The monkey then indicated its direction judgement with a saccade to one of the targets. On stimulation trials, FEF microstimulation began immediately upon fixation-point offset. **c**, Sample saccade trajectories from single trials (plotted in 2-ms intervals): ×, microstimulation following fixation; +, discrimination without microstimulation (two trials); small circles, discrimination with microstimulation (two trials). The two large, grey circles represent the targets. The fixation point is at the origin. **d**, Time courses of the numbered saccades in **c**. Thin and thick lines indicate horizontal (*x*) and vertical (*y*) positions, respectively. **e**, Latencies of first (electrically evoked) and second (voluntary) saccades measured with respect to fixation-point offset for all stimulation trials ($n = 37,611$).

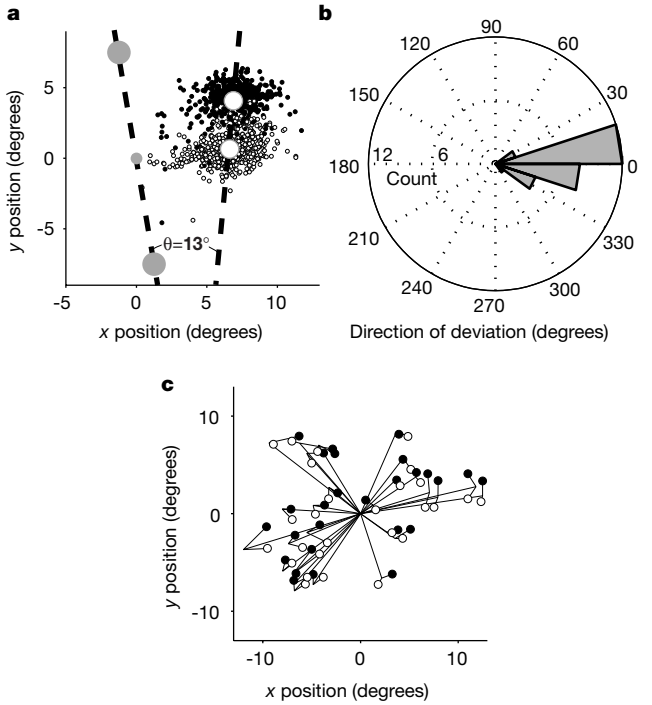

Figure 2 Effect of target choice on eye movements evoked electrically during the discrimination task. **a**, Evoked-saccade endpoints for all correct trials from the experiment shown in Fig. 1. Closed and open symbols represent upward and downward choices, respectively. White circles represent means of the two distributions of endpoints. Dashed lines through the mean endpoints and choice targets describe an angle θ, which compares the direction of saccade deviation to the direction of the motion discrimination. **b**, Distribution of angles (θ) for 27 microstimulation experiments. **c**, Mean endpoint positions of evoked saccades for all correct trials from each site tested. Line segments radiating from the origin represent the mean evoked saccade from fixation trials. Circles show the mean endpoints for evoked saccades from discrimination trials, sorted by the ensuing target choice. Filled circles indicate the more upward choice.

significant at each coherence: polynomial regression, $P < 0.01$). This result implies that dynamic signals present in the oculomotor system during the motion-viewing period reflect the accumulation of motion information over time.

Like the evoked saccades, the monkeys' behavioural performance depended on the strength and viewing duration of the motion stimulus (Fig. 4). We investigated whether the monkeys' performance could be governed by the same process that gives rise to the variation in the evoked saccades. The curves in Fig. 4 represent fits to the behavioural data of a model that predicts the probability of making a correct direction judgement for a given motion strength and viewing duration (equation (2) in Methods). This prediction is based on the difference between two variable quantities, S_c and S_i, which can be thought of as the accumulated responses of motion sensors that encode the correct and incorrect directions of motion, respectively:

$$\langle S_c \rangle = (r_0 + aC^m)T^n$$
$$\langle S_i \rangle = r_0 T^n \quad (1)$$

where $\langle \ldots \rangle$ denotes the expectation, C is coherence (0 to 1), T is viewing duration (in s) and r_0 is the response (in spikes s^{-1}) associated with 0% motion coherence. The remaining terms are fitted, positive-valued parameters: a and m parameterize the effects of coherence on the expected signals, and n describes a power law that governs how the signals accumulate in time. S_c and S_i, representing the accumulation of spikes, were treated as random variables with variances that scaled with their means[18,19]. For simplicity, only S_c depends on motion strength.

By adjusting the values of the free parameters in equation (1), we found a model that closely predicted the monkeys' ability to make a correct direction discrimination (Fig. 4). For both stimulation and non-stimulation trials, the best fit produced values of m and n that were near unity. These values imply that the monkeys' direction judgements are based on signals that scale in an essentially linear fashion with both coherence and viewing duration. The linear dependence on coherence mimics the responses of neurons in the middle temporal visual area (MT) to random-dot motion[20]. The linear dependence on time indicates that this type of coherence-dependent activity is temporally integrated to convert spike rate to an accumulated count, similar to the conversion of eye velocity to eye position in the brainstem[21].

The model of behavioural performance assumes that, on a given trial, the monkeys' decisions are based on the relative magnitudes of the signals defined in equation (1). When S_c is greater, the monkey chooses the actual direction of coherent motion. When S_i is greater, the monkey chooses the incorrect direction. The values of these signals, estimated from the behavioural data, are related to a quantity known as a decision variable, which describes the relative likelihood of one alternative versus another[1,2,22]. We found that a decision variable in the form of the log of the expected difference between S_c and S_i (equations (3) and (4) in Methods) bears a striking similarity to the magnitude of deviation measured in the evoked saccades (Fig. 5; χ^2 goodness of fit, $Q = 0.047$). For correct choices, both the decision variable and the saccade deviations increased with longer viewing duration and stronger motion. For incorrect choices, both quantities increased with longer viewing duration but decreased with greater motion strength.

The freedom to shift and scale the decision variable derived from performance does not trivialize its close agreement with the magnitude of saccade deviations at all motion strengths. For example, the freedom to adjust each of the solid curves independently did not significantly improve the fit ($P = 0.195$, likelihood ratio test). This result indicates that the coherence dependence of the decision variable is particularly important, even when scaled and shifted. We further assessed the significance of this dependence by fitting the deviation data with a model that was not based on the decision variable. We assumed that oculomotor commands could be initiated with different latencies depending on task difficulty but

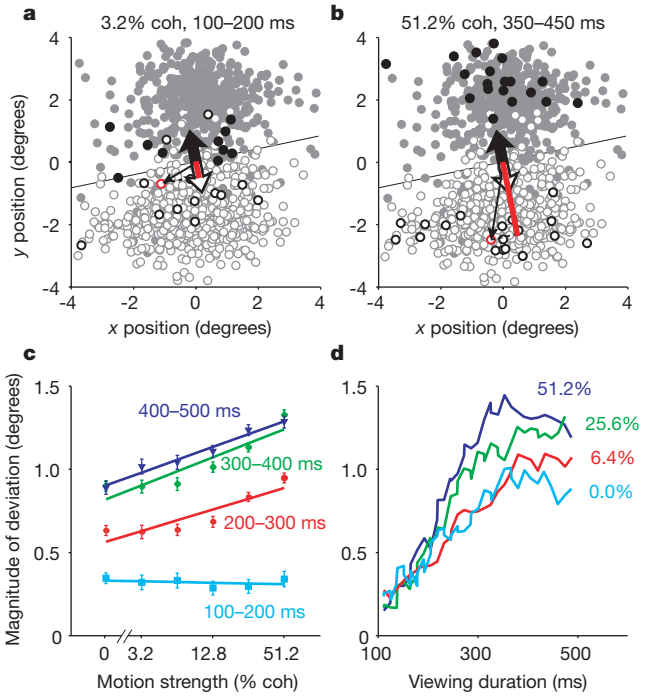

Figure 3 Effect of motion strength and viewing duration on eye movements evoked electrically during the discrimination task. **a**,**b**, Evoked-saccade endpoints from the experiment in Fig. 2a, corrected for drift during the experiment. The origin represents the average endpoint for both choices (see Methods). Deviation magnitude was quantified as the dot product between the endpoint vector (thin arrows) and the unit vector toward the chosen target (thick arrows). Examples are in red. Black lines indicate zero magnitude. coh, coherence. Deviation magnitude was smaller with weak motion and short viewing durations (bold symbols in **a**; mean ± s.e.m., 0.7 ± 0.2°) than with strong motion and longer durations (**b**; 2.4 ± 0.1°). **c**, Summary for 27 sites, data separated by viewing duration. Symbols and error bars represent mean ± s.e.m. **d**, Summary data separated by motion strength. Curves represent 300-point running means. Data in **a**–**d** are from correct trials.

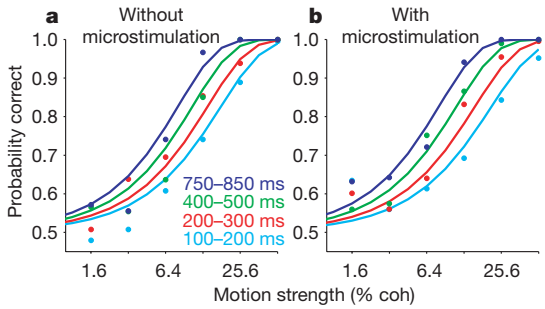

Figure 4 Behavioural performance as a function of motion strength and viewing duration. Viewing duration is binned into four groups, as indicated. Solid curves are maximum-likelihood fits to the behavioural data, derived from equations (1) and (2). **a**, Data from 14,481 non-microstimulation trials. For this fit, $a = 0.37$ spikes s^{-1} per percent coherence (95% confidence interval (CI): 0.29–0.48), $m = 1.04$ (CI: 0.95–1.12) and $n = 0.90$ (CI: 0.75–1.06). **b**, Data from 37,611 microstimulation trials. The monkeys indicated their choices with a voluntary saccade to one of the choice targets after the electrically evoked eye movement. For this fit, $a = 0.37$ spikes s^{-1} per percent coherence (CI: 0.32–0.43), $m = 1.03$ (CI: 0.98–1.13) and $n = 1.09$ (CI: 0.98–1.18). Although the fits in **a** and **b** differed significantly (likelihood-ratio test; $P < 0.0001$), they describe similar effects of motion strength and viewing duration on performance.

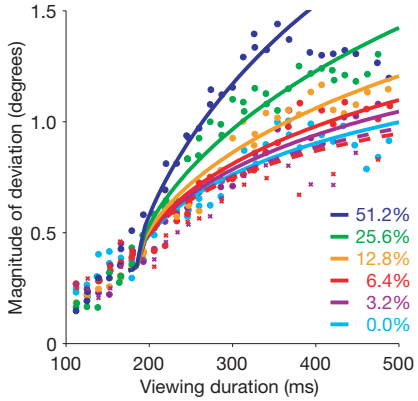

Figure 5 Comparison of the deviation of evoked saccades and a decision variable. Symbols represent the deviations of eye movements evoked electrically during the discrimination task in the direction of the chosen target (see Fig. 3d). These deviations are plotted as a function of viewing duration for different motion strengths, as labelled. Curves represent the logarithm of a decision variable inferred from the behavioural data in Fig. 4b. Filled circles and solid curves represent correct trials; crosses and dashed curves represent error trials.

then developed in a stereotyped manner (equation (5)), as might occur if the decision were computed first. This fit was poor (χ^2 goodness of fit, $Q < 10^{-14}$), unlike the model based on the decision variable (Fig. 5).

Note that for viewing durations of less than 184 ms (δ in equation (4)), motion strength did not affect the evoked saccades even though it did influence the monkeys' choices (Fig. 4). It therefore seems likely that the interpretation of motion information occurred in the time between the evoked and voluntary saccades. The saccade deviations before 184 ms may have reflected a predisposition to choose one of the saccade targets, as seen in physiological recordings from the lateral intraparietal area (LIP) and the superior colliculus[23,24]. For longer durations, the magnitude of saccade deviation appeared to plateau, perhaps reflecting an end to the linear accumulation of sensory information once a judgement was reached, even if motion viewing continued.

The close relationship between the deviations of evoked saccades and a decision variable inferred from behaviour indicates that developing oculomotor commands may reflect the formation of the monkey's direction judgement. Whether this means that the mechanisms responsible for generating the oculomotor commands are the same as those that generate the judgement is unclear. Decision formation could occur separately from motor preparation, in areas such as the superior colliculus, the prefrontal cortex or area LIP, each of which contains subsets of neurons that appear to be involved in the interpretation of visual motion information[24–26]. However, some (if not all) of these structures are undoubtedly involved in generating the oculomotor signals reflected in the evoked saccades and thus could take part in a direct conversion of motion information into an eye-movement command. Indeed, the ability to observe intermediate stages of decision formation in oculomotor signals seems implausible if the interpretation of motion information were completed elsewhere, as a fully formed judgement should elicit the same eye movement regardless of the information used to reach that judgement. It remains to be seen whether neural structures associated with the preparation of behavioural responses have a general role in the formation of perceptual judgements. □

Methods

Behavioural task

The motion stimulus was contained within a 5° circular aperture centred on the fixation point (Fig. 1a). On successive video frames, a percentage of randomly chosen dots moved towards one of two choice targets along the axis of motion discrimination (5° s^{-1}); the remainder of the dots were replotted at random locations. The percentage of coherently moving dots, viewing duration (100 ms plus a random time chosen from an exponential distribution with mean 200 ms) and direction were randomly interleaved. During motion viewing, the monkey maintained fixation within ±0.6° and did not make pursuit movements. The monkey received a liquid reward for a correct response (an eye movement to the target in the direction of coherent motion) and on half of the 0% coherence trials.

Electrophysiology

Monkeys were prepared for the microstimulation experiments by surgical implantation of an eye coil, head-holding device and recording cylinder. The FEF was targeted using stereotaxic information and magnetic resonance imaging, as described[26]. Electrical microstimulation consisted of a train of 0.25-ms-long, biphasic pulses applied at a rate of 350–450 Hz for 60 ms. A site was selected if saccades with consistent trajectories were evoked using <50 μA of current applied in darkness[27]. The axis of motion discrimination was then rotated to be roughly perpendicular to the trajectory of the evoked saccade, and the microstimulation current was adjusted to evoke saccades reliably during the motion-discrimination task (25–110 μA). In each experiment, 75% of the trials were accompanied by microstimulation.

All training, surgery and experimental procedures were in accordance with the National Institutes of Health Guide for the Care and Use of Laboratory Animals and were approved by the University of Washington Animal Care Committee.

Data analysis

Eye position was monitored using the scleral search-coil technique (sampled at 500 Hz)[28,29]. On stimulation trials, we included for analysis only trials in which two saccades were observed within 350 ms following microstimulation onset. Saccade endpoints were measured in a 20-ms epoch following the evoked saccade and preceding the monkey's voluntary saccade. Drift in endpoint position over the course of an experiment (lasting 2–4 h) was accounted for by subtracting a 300-point, chronological running mean from the endpoints. The magnitude of saccade deviation was quantified as the dot product between the vector from the fixation point to the saccade endpoint (corrected for drift) and the unit vector from the fixation point towards the target (see Fig. 3a, b). Deviation magnitude was computed only for trials with viewing durations ≤500 ms, because measurements from longer trials were sparse.

Fit to behavioural data

According to the model in equation (1), a correct response ensues when $S_c > S_i$. If the signals are independent and normally distributed, then the probability, P, of a correct response is

$$P(C,T) = \frac{1}{\sqrt{2\pi\sigma^2}} \int_0^\infty e^{-\frac{(x-\mu)^2}{2\sigma^2}} dx$$

$$\text{where} \quad \mu = \langle S_c \rangle - \langle S_i \rangle, \ \sigma^2 = (\langle S_c \rangle + \langle S_i \rangle)\phi \text{ and } \phi = \frac{Var[S_c]}{\langle S_c \rangle} = \frac{Var[S_i]}{\langle S_i \rangle} \tag{2}$$

The psychometric functions (Fig. 4) were derived by maximizing the (binomial) likelihood of observing the monkeys' choices: that is, $\underset{a,m,n}{\text{argmax}}\, L(choices|a, m, n)$. The values of ϕ (equation (2)) and r_0 (equation (1)) affect the estimate of a (equation (1)) but cause minimal changes from unity in the values of the exponents, m and n, when fit to the behavioural data. Confidence intervals were estimated by varying the fitted parameters to delimit an acceptance region for the null hypothesis (likelihood ratio test; χ^2, d.f. = 3, $P > 0.05$). We set $r_0 = 10$ spikes s^{-1}, which is consistent with measurements from area MT[20], and $\phi = 0.3$, a reasonable value for the pooled responses of weakly correlated neurons[11,30]. These values yielded $a = 0.37$ spike s^{-1} per percent coherence, which is in close agreement with values reported for area MT[20].

Decision variable

The fit of equations (1) and (2) enabled us to derive a decision variable, D, based on a comparison of S_c and S_i:

$$D(C,T) = \begin{cases} \langle S_c - S_i | S_c > S_i \rangle & \text{correct choice} \\ \langle S_i - S_c | S_i > S_c \rangle & \text{incorrect choice} \end{cases} \tag{3}$$

where $\langle x|y \rangle$ indicates the expected value of x under the condition y. D is the expected difference between S_c and S_i, computed separately for correct and incorrect choices. Note that D is always positive.

We fit the measured deviations of electrically evoked saccades with a scaled version of the logarithm of the decision variable, D:

$$f(C,T) = \beta \log[1 + D(C, T - \delta)] + h(T) \tag{4}$$

where β and δ are free parameters representing a scaling factor and a delay, respectively. For $T < \delta$, the fit is dominated by $h(T)$, a time-dependent offset that is modelled as a saturating exponential with a short time constant, $\tau \ll \delta$. The best alignment (least squares) was achieved using $\beta = 0.69$ and $\delta = 184$ ms (Fig. 5). The particular form of the function is probably unimportant beyond the qualitative observation that D, compressed and shifted, matches the family of eye-movement curves obtained by microstimulation. We also fit the

data in Fig. 5 with an alternative model, in which the saccade deviation arises from stereotyped dynamics of oculomotor commands that are simply delayed as a function of motion strength:

$$f(C,T) = \alpha + \beta\left[1 - e^{-\left(\frac{T-\delta_C}{\tau}\right)^n}\right] \quad (5)$$

The free parameters α, β, τ and n describe the temporal dynamics of the saturating exponential function, independent of motion strength. Only the delay term, δ_c, varied with motion strength.

Received 15 October 1999; accepted 26 January 2000.

1. Graham, N. V. S. *Visual Pattern Analyzers* (Oxford Univ. Press, Oxford, 1989).
2. Carpenter, R. H. & Williams, M. L. Neural computation of log likelihood in control of saccadic eye movements. *Nature* **377,** 59–62 (1995).
3. Leon, M. I. & Shadlen, M. N. Exploring the neurophysiology of decisions. *Neuron* **21,** 669–672 (1998).
4. Schall, J. D. & Thompson, K. G. Neural selection and control of visually guided eye movements. *Annu. Rev. Neurosci.* **22,** 241–259 (1999).
5. Britten, K. H., Shadlen, M. N., Newsome, W. T. & Movshon, J. A. The analysis of visual motion: a comparison of neuronal and psychophysical performance. *J. Neurosci.* **12,** 4745–4765 (1992).
6. Schlag-Rey, M., Schlag, J. & Shook, B. Interactions between natural and elecrically evoked saccades. I. Differences between sites carrying retinal error and motor error signals in monkey superior colliculus. *Exp. Brain Res.* **76,** 537–547 (1989).
7. Kustov, A. A. & Robinson, D. L. Shared neural control of attentional shifts and eye movements. *Nature* **384,** 74–77 (1996).
8. Sparks, D. L. & Mays, L. E. Spatial localization of saccade targets. I. Compensation for stimulation-induced perturbations in eye position. *J. Neurophysiol.* **49,** 45–63 (1983).
9. Sparks, D. L., Mays, L. E. & Porter, J. D. Eye movements induced by pontine stimulation: interaction with visually triggered saccades. *J. Neurophysiol.* **58,** 300–318 (1987).
10. Tehovnik, E. J., Slocum, W. M. & Schiller, P. H. Behavioural conditions affecting saccadic eye movements elicited electrically from the frontal lobes of primates. *Eur. J. Neurosci.* **11,** 2431–2443 (1999).
11. Shadlen, M. N., Britten, K. H., Newsome, W. T. & Movshon, J. A. A computational analysis of the relationship between neuronal and behavioral responses to visual motion. *J. Neurosci.* **16,** 1486–1510 (1996).
12. Bruce, C. J. & Goldberg, M. E. Primate frontal eye fields. I. Single neurons discharging before saccades. *J. Neurophysiol.* **53,** 603–635 (1985).
13. Wurtz, R. H. & Goldberg, M. E. Activity of superior colliculus in behaving monkey. III. Cells discharging before eye movements. *J. Neurophysiol.* **35,** 575–586 (1972).
14. Mays, L. E. & Sparks, D. L. Dissociation of visual and saccade-related responses in superior colliculus neurons. *J. Neurophysiol.* **43,** 207–232 (1980).
15. Schiller, P. H. & Sandell, J. H. Interactions between visually and electrically elicited saccades before and after superior colliculus and frontal eye field ablations in the rhesus monkey. *Exp. Brain Res.* **49,** 381–392 (1983).
16. Lee, C., Rohrer, W. H. & Sparks, D. L. Population coding of saccadic eye movements by neurons in the superior colliculus. *Nature* **332,** 357–360 (1988).
17. Sparks, D. L., Lee, C. & Rohrer, W. H. Population coding of the direction, amplitude, and velocity of saccadic eye movements by neurons in the superior colliculus. *Cold Spring Harb. Symp. Quant. Biol.* **55,** 805–811 (1990).
18. Geisler, W. S. & Albrecht, D. G. Visual cortex neurons in monkeys and cats: detection, discrimination, and identification. *Vis. Neurosci.* **14,** 897–919 (1997).
19. Shadlen, M. N. & Newsome, W. T. The variable discharge of cortical neurons: implications for connectivity, computation, and information coding. *J. Neurosci.* **18,** 3870–3896 (1998).
20. Britten, K. H., Shadlen, M. N., Newsome, W. T. & Movshon, J. A. Responses of neurons in macaque MT to stochastic motion signals. *Vis. Neurosci.* **10,** 1157–1169 (1993).
21. Robinson, D. A. Integrating with neurons. *Annu. Rev. Neurosci.* **12,** 33–45 (1989).
22. Green, D. M. & Swets, J. A. *Signal Detection Theory and Psychophysics* (Wiley, New York, 1966).
23. Platt, M. L. & Glimcher, P. W. Neural correlates of decision variables in parietal cortex. *Nature* **400,** 233–238 (1999).
24. Horwitz, G. D. & Newsome, W. T. Separate signals for target selection and movement specification in the superior colliculus. *Science* **284,** 1158–1161 (1999).
25. Shadlen, M. N. & Newsome, W. T. Motion perception: seeing and deciding. *Proc. Natl Acad. Sci. USA* **93,** 628–633 (1996).
26. Kim, J.-N. & Shadlen, M. N. Neural correlates of a decision in the dorsolateral prefrontal cortex of the macaque. *Nature Neurosci.* **2,** 176–185 (1999).
27. Bruce, C. J., Goldberg, M. E., Bushnell, M. C. & Stanton, G. B. Primate frontal eye fields. II. Physiological and anatomical correlates of electrically evoked eye movements. *J. Neurophysiol.* **54,** 714–734 (1985).
28. Robinson, D. A. A method of measuring eye movement using a scleral search coil in a magnetic field. *IEEE Trans. Biomed. Eng.* **10,** 137–145 (1963).
29. Judge, S. J., Richmond, B. J. & Chu, F. C. Implantation of magnetic search coils for measurement of eye position: an improved method. *Vision Res.* **20,** 535–538 (1980).
30. Zohary, E., Shadlen, M. N. & Newsome, W. T. Correlated neuronal discharge rate and its implications for psychophysical performance. *Nature* **370,** 140–143 (1994).

Acknowledgements

We thank M. Mihali for animal training and technical support, and E. Freedman, G. Horwitz, B. Jagadeesh, T. Movshon and F. Rieke for helpful comments on the manuscript. This work was supported by the NEI, NCRR and the McKnight Foundation.

Correspondence and requests for materials should be addressed to M.N.S. (e-mail: shadlen@u.washington.edu).

A *Drosophila* model of Parkinson's disease

Mel B. Feany* & Welcome W. Bender†

** Department of Pathology, Division of Neuropathology, Brigham and Women's Hospital and Harvard Medical School, and †Department of Biological Chemistry and Molecular Pharmacology, Harvard Medical School, Boston, Massachusetts 02115, USA*

Parkinson's disease is a common neurodegenerative syndrome characterized by loss of dopaminergic neurons in the substantia nigra, formation of filamentous intraneuronal inclusions (Lewy bodies) and an extrapyramidal movement disorder. Mutations in the α-*synuclein* gene are linked to familial Parkinson's disease[1,2] and α-synuclein accumulates in Lewy bodies and Lewy neurites[3–5]. Here we express normal and mutant forms of α-synuclein in *Drosophila* and produce adult-onset loss of dopaminergic neurons, filamentous intraneuronal inclusions containing α-synuclein and locomotor dysfunction. Our *Drosophila* model thus recapitulates the essential features of the human disorder, and makes possible a powerful genetic approach to Parkinson's disease.

It is unclear how mutations in α-synuclein, an abundant neuronal protein of unknown function, produce neurodegeneration in familial cases of Parkinson's disease. However, the dominant inheritance pattern and production of insoluble protein aggregates indicate a toxic dominant mechanism, perhaps relating to abnormal protein accumulation. Expression of human α-synuclein in *Drosophila* might therefore model Parkinson's disease. We have produced transgenic fly lines that produce normal human α-synuclein and separate lines with each of the two mutant proteins linked to familial Parkinson's disease, A30P and A53T α-synuclein.

We use a bipartite expression system that relies on transcriptional activation by the yeast protein GAL4 (ref. 6) to express normal and mutant α-synuclein in flies. Normal and mutant human α-synuclein complementary DNA constructs are placed downstream of multiple binding sites for GAL4. Transgenic animals carrying the GAL4-responsive constructs are then crossed to a number of well characterized lines that express the yeast activator in a variety of tissue- and cell-type-specific patterns (the 'drivers'). Development of neuronal and non-neuronal tissues proceeds normally in the presence of human α-synuclein, as indicated by appropriate external morphology, histological appearance (Fig. 1a, b), viability and behaviour of newly eclosed flies (Table 1). To confirm appropriate activity of the drivers, we expressed an unrelated toxic protein, mutant ataxin-1, in the same developmental and tissue-specific patterns. In contrast to α-synuclein, mutant ataxin-1 produces marked defects during development (Table 1). Other laboratories have also induced phenotypes with these driver lines[7].

The nervous system is appropriately formed in α-synuclein transgenic flies, and the aging brain shows no widespread degenerative changes (Fig. 1a, b). Overall brain volume is likewise preserved in many patients with Parkinson's disease, but marked degeneration occurs in specific groups of neurons. Dopaminergic neurons are preferentially lost in Parkinson's disease; we therefore examined dopaminergic neurons in α-synuclein transgenic flies. We used multiple independent markers to identify dopaminergic cells.

First, we stained serial tissue sections through the entire brain of the adult fly with an antibody against tyrosine hydroxylase, which specifically identifies dopaminergic neurons. The position and arrangement of dopaminergic neurons in the developing and adult *Drosophila* nervous system has been documented in detail[8–10]. Tyrosine hydroxylase immunostaining shows a prominent cluster of dopaminergic neurons (the dorsomedial group) that is